Univerzita Karlova v Praze

Matematicko-fyzikální fakulta

BAKALÁŘSKÁ PRÁCE

Michael Pešek

Low temperature proton polarized target for nucleon structure studies at COMPASS

Katedra fyziky nízkých teplot

Vedoucí bakalářské práce: prof. Ing. Miroslav Finger, DrSc.

Studijní program: Fyzika

Studijní obor: Obecná fyzika

Praha 2012

Charles University in Prague

Faculty of Mathematics and Physics

BACHELOR THESIS

Michael Pešek

Low temperature proton polarized target for nucleon structure studies at COMPASS

Department of Low Temperature Physics

Supervisor of the bachelor thesis: prof. Ing. Miroslav Finger, DrSc.

Study programme: Physics

Specialization: General physics

Prague 2012

I would like to express my thanks to my supervisor prof. Finger for giving me the possibility of doing my thesis at COMPASS. Then I would like to thank several members of COMPASS collaboration for their help, namely Jaakko H. Koivuniemi and Kaori Kondo from the polarised target group. Special thanks belong to my friend Kateřina Srbecká for her help with the language side of my thesis. Last but not least thanks belong to my friend Petr Veřtát for his extraordinary moral and emotional support which helped me very much with my work.

Prohlašuji, že jsem tuto bakalářskou práci vypracoval samostatně a výhradně s použitím citovaných pramenů, literatury a dalších odborných zdrojů.

Beru na vědomí, že se na moji práci vztahují práva a povinnosti vyplývající ze zákona č. 121/2000 Sb., autorského zákona v platném znění, zejména skutečnost, že Univerzita Karlova v Praze má právo na uzavření licenční smlouvy o užití této práce jako školního díla podle § 60 odst. 1 autorského zákona.

I declare that I carried out this bachelor thesis independently, and only with the cited sources, literature and other professional sources.

I understand that my work relates to the rights and obligations under the Act No. 121/2000 Coll., the Copyright Act, as amended, in particular the fact that the Charles University in Prague has the right to conclude a license agreement on the use of this work as a school work pursuant to Section 60 paragraph 1 of the Copyright Act.

V Praze dne/In Prague, date ..... Podpis autora/signature

……..

Název práce: Nízkoteplotní protonový polarizovaný terč pro studium struktury nukleonů v experimentu COMPASS

Autor: Michael Pešek

Katedra / Ústav: Katedra fyziky nízkých teplot

Vedoucí bakalářské práce: prof. Ing. Miroslav Finger, DrSc., Katedra fyziky nízkých teplot

Abstrakt: V této práci jsou prezentovány základní přehledy hlubokého nepružného rozptylu a procesu dynamické jaderné polarizace. Je kladen důraz na důležidost určení polarizace pro studium spinové struktury nukleonu. Následuje popis experimentu COMPASS s důrazem na popis nízkoteplotního polarizovaného terče. Je popsána obecná procedura pro určení polarizace a určena polarizace a relaxační doby pro běh experimentu v roce 2010.

Klíčová slova: struktura nukleonu, polarizovaný protonový terč, nízké teploty, metoda NMR

Title: Low temperature proton polarized target for nucleon structure studies at COMPASS

Author: Michael Pešek

Department / Institute: Department of Low temperature Physics

Supervisor of the bachelor thesis: prof. Ing. Miroslav Finger, DrSc., Department of Low Temperature Physics

Abstract: Overview of basics of deep inelastic scattering and process of dynamic nuclear polarization with emphasis to importance of precise polarization determination for nucleon spin structure studies are given. This is followed by description of COMPASS experiment with emphasis given to low temperature polarized target. General procedure of NMR data analysis is given and finally polarization for run 2010 and relaxations rates are determined.

Keywords: nucleon structure, polarized proton target, low temperatures, NMR technique

Contents

Introduction

In 1988 EMC (European Muon Collaboration) discovered that quarks in nucleons contribute only by small fraction to overall spin of nucleon (see [1]) This lead naturally to further studies of nucleon structure in order to resolve this puzzle. One of experiments designed to study nucleon structure is COmmon Muon and Proton Apparatus for Structure and Spectroscopy (COMPASS) experiment approved at CERN in 1997 and which started data taking in 2002. Its two main goals were to perform hadron spectroscopy a study of nucleon structure via polarized Deep Inelastic Scattering (DIS) of muons on polarized target made of deuterated lithium ^{6}LiD and later also ammonia NH_3. In 2011 COMPASS – II was approved. It will continue further to study nucleon structure using Deeply Virtual Compton Scattering and polarized Drell-Yan. More information can be found in COMPASS – II proposal [2].

The main goal of this thesis is to describe general procedure of measurig polarization of polarized target which is very important for measuring polarized DIS and polarized Drell-Yann in future also.

1. Physics of COMPASS experiment

1.1. Deep inelastic scattering – studying nucleon structure

Scattering of "somethig on something" has been used very often as method for studying structure of matter. (See neutron scattering or X-ray diffraction as one of the most often used examples.)

Now, let's take a look at inelastic scattering of lepton with four-momentum p on nucleon which is in rest. (This of course very broad topic, so only basic insights are given with respect to the main subject of this thesis.) This process can be described by formula (1.1.1).

$$\ell^{\pm} + n \rightarrow \ell^{\pm} + n + X \tag{1.1.1}$$

Where X denotes arbitrary particles created from the lost energy of the lepton. Denote the four-momentum of scattered muon by p' and is scattered at an angle θ. Following variable can be defined

$$Q^2 = -(p - p')^2 = -q^2, \tag{1.1.2}$$

where q^2 coresponds to square of transferred four-momentum. Then two other variables can be defined (definitions are valid in laboratory system)

$$\nu = \frac{p \cdot q}{m_n} = E - E' \tag{1.1.3}$$

and

$$x = \frac{Q^2}{2m_n \nu} \quad (0 \le x \le 1)), \tag{1.1.4}$$

where E respectively E' coresponds to energy of the initial lepton resp. scattered lepton. The x is so called Bjorken's x. (see [3]) Differential cross section for lepton scattered in solid angle Ω with energy E' can be expressed by following formula (see e.g. [4]):

$$\frac{d^2\sigma_{unpol}}{dE'\,d\Omega} = \frac{4\alpha^2 E'^2}{Q^4}\left(\frac{2F_1(x,Q^2)}{m_n}\sin^2\frac{\theta}{2} + \frac{F_2(x,Q^2)}{\nu}\cos^2\frac{\theta}{2}\right), \tag{1.1.5}$$

where $F_1(x, Q^2)$ *and* $F_2(x, Q^2)$ are so called *unpolarized structure functions (sometimes called spin-independent strucure functions)* and α is electromagnetic constant of fine structure. Structure functions are related to parton distribution functions, which give probability density for finding a parton carrying fraction of momenta of nucleon x at momentum transfer Q^2.

Now let's consider polarized case i.e. polarized both lepton and nucleon. The difference between cross sections of opposite nucleon spin is given by following formula (for example [4]):

$$\frac{d^2\sigma(\beta)}{dE'\,d\Omega} - \frac{d^2\sigma(\beta+\pi)}{dE'\,d\Omega} = \frac{4\alpha^2 E'}{Q^2 m_n E}\left[\begin{array}{l} g_1\left(x,Q^2\right)\cdot\left(E\cos\beta + E'\cos\psi\right) \\ + g_2\left(x,Q^2\right)\dfrac{2EE'}{\nu}\cdot\left(\cos\psi - \cos\beta\right)\end{array}\right], \qquad (1.1.6)$$

where β is angle between the direction of incoming lepton and spin of nucleon (in lab system), $\cos\psi = \sin\theta\sin\beta\cos\phi + \cos\theta\cos\beta$ and ϕ is azimutal angle between scattering plane and nucleon polarization plane. And $g_1(x, Q^2)$ and $g_2(x, Q^2)$ are so called *polarized structure functions (*also called *spin-dependent strucure functions).*

We now consider two cases with β=0 and β=π/2, which are interesting from experimental poin of view. Case β=0 corresponds to situation in which the lepton spin is parallel (⇉) or antiparallel (⇄) to the spin of nucleon and formula (1.1.6) is simplified to

$$\frac{d^2\Delta\sigma_{\parallel}}{dE'\,d\Omega} \equiv \frac{d^2\sigma^{\overrightarrow{\leftarrow}}}{dE'\,d\Omega} - \frac{d^2\sigma^{\overrightarrow{\rightarrow}}}{dE'\,d\Omega} = \frac{4\alpha^2 E'}{Q^2 m_n E}\left[g_1\cdot\left(E + E'\cos\theta\right) + g_2\cdot\frac{Q^2}{\nu}\right]. \qquad (1.1.7)$$

The second case with β=π/2 corresponds to situation where nucleon spin is perpendicular to the spin of lepton and (1.1.6) changes to

$$\frac{d^2\Delta\sigma_{\perp}}{dE'\,d\Omega} \equiv \frac{d^2\sigma^{\overrightarrow{\downarrow}}}{dE'\,d\Omega} - \frac{d^2\sigma^{\overrightarrow{\uparrow}}}{dE'\,d\Omega} = \frac{4\alpha^2 E'^2}{Q^2 m_n \nu}\frac{\sin\theta\cos\phi}{E}\left[g_1 + g_2\cdot\frac{2E}{\nu}\right]. \qquad (1.1.8)$$

Because of ϕ dependance and because polarized contributions to total cross section are small compared to unpolarized cross section determining of structure functions g_1 and g_2 is not too much practical experimentaly. Instead what is avaiable experimentally very well are the *spin asymmetries* $A_{||}$ and $A_{\perp}$ defined by following relations:

$$A_{\parallel} = \frac{\dfrac{d^2\Delta\sigma_{\parallel}}{dE'\,d\Omega}}{2\dfrac{d^2\sigma_{unpol}}{dE'\,d\Omega}} \text{ and } A_{\perp} = \frac{\dfrac{d^2\Delta\sigma_{\perp}}{dE'\,d\Omega}}{2\dfrac{d^2\sigma_{unpol}}{dE'\,d\Omega}}. \qquad (1.1.9)$$

Those are related to so called *photoabsorption asymmetries A_1 and A_2* (which are related to the fact that electromagnetic interaction between charged lepton and

partons in nucleon can be explained by exchange of virtual photon, see for example [4] or [5]) by following relations:

$$A_{\parallel} = a\left(A_1 + bA_2\right) \text{ and } A_{\perp} = c\left(A_2 + dA_1\right), \tag{1.1.10}$$

where the coeficients *a*, *b*, *c* and *d* are given by kinematics of the scattering process. Most important fact is that these asymmetries are related to structure functions g_1, g_2, F_1 by following formulas:

$$A_1\left(x,Q^2\right) = \frac{g_1 - \frac{Q}{\nu} g_2}{F_1} \text{ and } A_2\left(x,Q^2\right) = \frac{\frac{Q^2}{\nu^2}\left(g_1 + g_2\right)}{F_1}. \tag{1.1.11}$$

So finally by measuring $A_{||}$ and $A_{\perp}$ one can determine A_1 and A_2 and subsequently the structure functions. Now the polarization of the target comes in place, because everything up to now was considered in ideal state where both the beam and the nucleon are completely polarized, but in reality this is not the case. So experimentally measured spin asymmetries are related to the ideal asymmetries by following simple relations:

$$A_{\parallel}^{\text{exp}} = A_{\parallel} \cdot P_T \cdot P_B \cdot f \text{ and } A_{\perp}^{\text{exp}} = A_{\perp} \cdot P_T \cdot P_B \cdot f\,, \tag{1.1.12}$$

where P_T is the polarization of the target, P_B is the polarization of the beam and f is the dilution factor, i.e. fraction of polarizable nucleons in the target material.

The measurement of the assymetries and consequently the spin-dependent structure functions leads to possibility of determining the spin structure of nucleon. The spin of nucleon consists of several contributions

$$\frac{1}{2} = \frac{1}{2}\Delta\Sigma + \Delta G + L\,, \tag{1.1.13}$$

where $\Delta\Sigma$ is contrinution from spin of quarks, ΔG contribution from gluons and L is angular momentum of both quarks and gluons. As mentioned in the Introduction the EMC collaboration measured the contribution of quarks to be 0,128±0,013±0,019.

1.2. Dynamic nuclear polarization

As can be clearly seen in formula (1.1.12) the high target polaraization is necessary for measurement of the asymmetries. We will now describe the basic principles behind the *dynamic nuclear polarization* (DNP), focusing on systems with spin ½, in our case that means protons in NH_3. (More detailes can be found in [5] or in "bible" of nuclear magnetism [6].)

One of key requirements is that the material we want to polarize has to have paramagnetic centers i.e. unpaired electrons, which have hifh magnetic moment and therefore polarization of unpaired electrons is higher than 90%. The fundamental idea is then to transfer the high electron polarization to nuclear spins (in our case protons).

If we consider ensemble of particles with spin ½ we can define the polarization of such ensemble by following formula

$$P = \frac{n_+ - n_-}{n_+ + n_-}, \tag{1.2.1}$$

where n_+ is number of particles with *z*-projection of spin +½ and n_- number of particles with z-projection of spin -½.

If the system is in state of *thermal equilibrium* with the lattice, then the spins obey Boltzmann statistics. Zeeman splitting into two sublevels will occur if the ensemble is placed in external magnetic field B_0 pointing in z-axis. These two levels are separated by energy $\hbar\omega_0$, where ω_0 is Larmor frequency given by following relation

$$\omega_0 = \gamma \cdot B_0, \tag{1.2.2}$$

where γ is gyromagnetic ratio and which coresponds to frequency by which the spins precede in the magnetic field B_0. The polarization of the system in thermal equilibrium state can be calculated by the Brillouin function

$$P(x) = \frac{1}{I}\left[\left(I + \frac{1}{2}\right)\coth\left(\left(I + \frac{1}{2}\right)x\right) - \frac{1}{2}\coth\left(\frac{x}{2}\right)\right], \tag{1.2.3}$$

where I is the nuclear spin and

$$x = \frac{\hbar\omega_0}{k_B T}, \tag{1.2.4}$$

where k_B is Boltzmann constant and T is temperature. In our case where I=½ the formula (1.2.3) is simplified

$$P = \tanh\left(\frac{\hbar\omega_0}{2k_B T}\right). \tag{1.2.5}$$

The Zeeman splitting creates following four eigen-states

$$|++\rangle, |+-\rangle, |-+\rangle \text{ and } |--\rangle\ , \tag{1.2.6}$$

Because we have spin ½ particles + and – corresponds to +½ or -½ projection of spin of both nucleon (i.e. proton) and electron. Now, if we irradiate this system by radiofrequency field described by the following Hamiltonian

$$H_{rf} = \frac{\hbar\omega}{2} e^{-i\omega t} \tag{1.2.7}$$

then we can calculate the transition rate from state *i* to state *k* (i.e. the rate of spin flip) using Fermi's golden rule (see [7])

$$W_{i\to f} = \frac{2\pi}{\hbar} \left| \left\langle H_{rf} \right\rangle \right|^2 \delta(\left| E_i - E_f \right| - \hbar\omega) \tag{1.2.8}$$

This clearly shows that it's impossible to gain any polarization, because transition rate are same in both directions i.e. $i \to f$ and $f \to i$. Also the simultaneous flips of both nuclear spin and electron spin are impossible as such transition rate is zero.

To allow polarization buildup one has to consider dipole-dipole interactions between nucleon and electron. Such interaction can be described by following Hamiltonian (see [8])

$$H_{DD} = -\frac{\mu_0}{4\pi} \gamma_s \gamma_N \hbar^2 \left[\left(\vec{I} \cdot \vec{S} \right) - 3 \left(\vec{I} \cdot \vec{n} \right) \left(\vec{S} \cdot \vec{n} \right) \right] \frac{1}{r^3}, \tag{1.2.9}$$

where γ_s, γ_N are gyromagnetic ratios of electron and nucleus, $\vec{S}$ and $\vec{I}$ are spins of electron and nucleus and if the nucleus is at the origin of coordinate system then the $\vec{n}$ is unit vector conecting the nucleus and electron.

Now, if one calculates the new eigen-states using first order pertubation theory and new eigen-energies, then the dipole-dipole interaction leads to possibility of simultaneus flips of both the nuclear and electron spins. (Detailes on this rather nontrivial calculation can be found in [5] or [6], as providing detailed calculations is not goal of this brief introduction.) The main result is that the simultaneous flips are possible by iradiating the system by rf field with the following frequencies

$$\begin{aligned} \omega_+ &= \omega_e - \omega_N \\ \omega_- &= \omega_e + \omega_N \end{aligned}, \tag{1.2.10}$$

where ω_e is the Larmor frequency of electrons and ω_N is Larmor frequency of nucleus and indices + or – denotes whether this leads to positive polarization or negative polarization.

When the simultaneous flip of spins occur then, because of their huge mass difference, the electron relaxes much faster than the nucleus and other simultaneous

flip between electron and other nucleus can occur then this naturally leads to polarization buildup. Now it is also clear why one needs the unpaired electrons (alias paramagnetic centers). Only unpaired electrons can couple to nucleus and undergo simultaneous flip of spins.

One last effect deserves mentioning and that is so called *spin diffusion*. Because of strong dependence of the dipole-dipole interactions on distance, upaired electron can couple only to the nearest nuclei, but because interaction between nuclei also exists flip of spin of one nucleus can also flip spin of other nucleus - so the polarization literary diffuse through the system and leads to homogenous polarization even with rather small concentration of paramagnetic centers.

1.3. Measurement of polarization by NMR technique

In this section the basic principles and features of NMR method used for the polarization measurement will be described. More general and detailed information can be found in literature e.g. [8].

Consider the situation from previous section i.e. ensemble of nuclei in external static magnetic field B_0 which is pointing in z-axis. Such ensemble has a magnetization which is proportional to the external field

$$M = \chi_0 B_0 , \tag{1.3.1}$$

where χ_0 is so called static susceptibility. The magnetization M is also related to the polarization P by following formula

$$M = \mu N P , \tag{1.3.2}$$

where N is number of nuclei in the unit volume and μ is magnetic moment asociated with the spin of nucleus. NMR technique can be used to measure the nuclear susceptibility χ, which is linked to the polarization by formulas (1.3.1) and (1.3.2).

When the a rf signal is imposed onto the magnetic field B_0 then the susceptibility will no longer be a constant, but it will depend on frequency of the rf field and also it will have both real and imaginary parts

$$\chi(\omega) = \chi'(\omega) - i\chi''(\omega), \tag{1.3.3}$$

where χ' is so called dispersion function and χ'' is so called absorption function. These of course satisfy famous Kramers-Krönig relations (see [9])

$$\chi'(\omega) = \frac{1}{\pi} P\int_{-\infty}^{+\infty} \frac{\chi''(\omega')}{\omega' - \omega} d\omega' \text{ and } \chi''(\omega) = -\frac{1}{\pi} P\int_{-\infty}^{+\infty} \frac{\chi'(\omega')}{\omega' - \omega} d\omega' . \tag{1.3.4}$$

Because $\chi'(0) \equiv \chi_0$ then from formulas (1.3.1), (1.3.2) and (1.3.4) one can clearly see that the polarization is proportional to the integral of absorbtion function

$$P \propto \int \frac{\omega_0 \chi''(\omega')}{\omega'} d\omega', \tag{1.3.5}$$

where ω_0 is Larmor frequency defined by (1.2.2). Now the absorbtion function can be actually measured by measuring the change of NMR coil inductance L, which depends on susceptibility by following formula (see [10])

$$L(\omega) = L_0[1 + \mu_0 \eta \chi(\omega)], \tag{1.3.6}$$

where μ_0 is permeability of vacuum, η is so called effective filling factor i.e. ratio of target material volume inside the coil and the coil volume and L_0 is inductance of the empty coil. This can be measured by RLC circuit and it leads to the NMR signal voltage proportional to absorbtion function

$$V_{NMR}(\omega) \propto \chi''(\omega). \tag{1.3.7}$$

Because the width of the NMR signal of protons is much smaller than the Larmor frequency of protons ω_0 (few hundreds kHz versus 106 MHz) the (1.3.5) can be simplified to

$$P \propto \int \chi''(\omega) d\omega. \tag{1.3.8}$$

From (1.3.7) and (1.3.8) now follows that the polarization value is proportional to area of NMR signal S_{NMR}

$$P = CS_{NMR}. \tag{1.3.9}$$

The constant C can be termined using thermal equilibrium polarization P_{TE}. Because the P_{TE} can be calculated analytically by formula (1.2.5) then the constant C can be calculated by

$$C = \frac{P_{TE}}{S_{TE}}, \tag{1.3.10}$$

where S_{TE} is area of the NMR signal at thermal equilibrium.

For the analysis purpose it is also useful that the susceptibility at temperatures used for thermal equilibrium calibration (and consequently the polarization) follow the Curie law (see [8]) which consequently applies to the NMR signal area

$$S_{TE} = \frac{C_{curie}}{T}. \tag{1.3.11}$$

2. COMPASS Experiment at CERN

2.1. General description

COMPASS experiment is fixed target experiment located in building 888 at CERN and is using M2 secondary beam¨line which provides muon and hadron beams for nucleon structure studies and hadron spectrocopy. Momentum of muon beam can be slected between 60 GeV/c and 190 GeV/c and 160GeV/c is standartely used. The polarization of the muon beam was measured to be (-80±4) % and maximum allowed flux is 2.10^8 per spill, which lasts 4,8 s. (See [11].) Momentum of hadron beam can be selected up to 280GeV/c. The particle identification of the beam paricles is done by two differential Cherenkov counters (CEDAR).

Fig. 2.1.1(taken from [2]) shows top view of COMPASS spectrometer in configuration used in 2010.

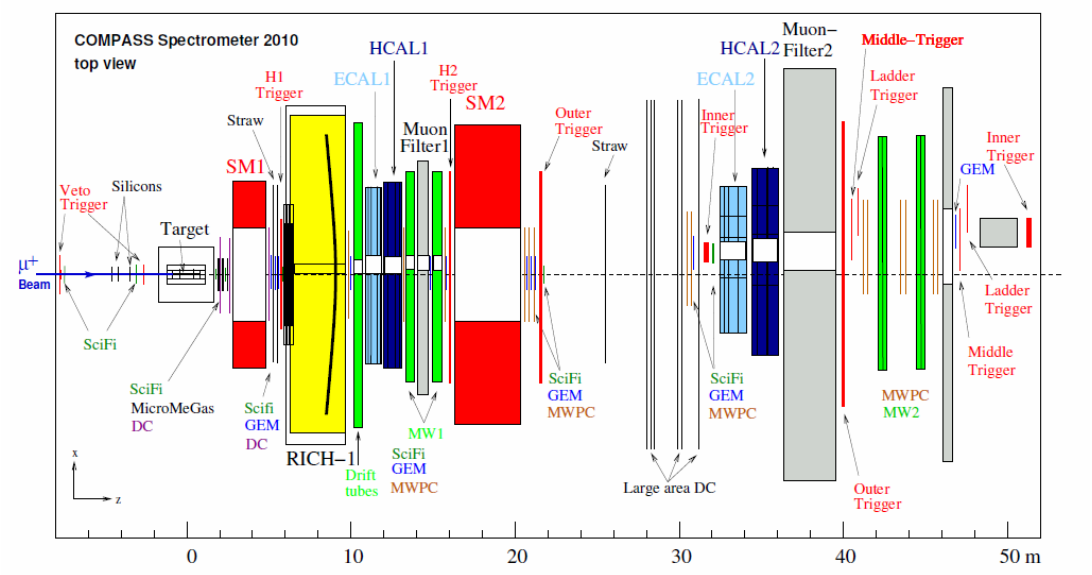

Figure 2.1.1 - Top view of spectrometer

As can be seen from picture, COMPASS is two-stage spectrometer consisting of the so called Large Angle Spectrometer (LAS) and Small Angle Spectrometer (SAS) with target platform situated in the beginning of LAS. The platform can cary both the solid targets for hadron spectroscopy and mainly the polarized target used with muon beam (and also LH_2 target for future DVCS studies) which will be describe in details in next section.

The LAS is centered around the SM1 magnet and has both particle idenfication by RICH detector and both electromagnetic and hadronic calorimeters along with several drift chambers, multi-wire proportional chambers and several other path detectors.

The SAS follows behind the SM2 magnet and has again both electromagnetic and hadronic calorimeters along with drift chambers, muon chambers and straw detectors. Detailed description of both beam line and detectors of which the spectrometer consists can be found in [11].

2.2. Polarized target

Polarized target is the key component of the COMPASS experiment. It's one of the components which make COMPASS rather unique, so it deserves detailed description. Fig. 2.2.1 presents general view of the target. The target consists of three cells with diameter of 3 centimeters. Both upstream and downstream cells are 30 cm long and middlestream cell is 60 cm long. During 2010 and 2011 runs solid ammonia was used as target material. Each cell contains several NMR coils – 3 are for upstream and 3 for downstream cells and 4 are for middlestream cell. In total 10 NMR coils are used. These three cells are placed in microwave cavity which alows polarization build up using microwave signals (see section 1.2. for principles of polarization build up). The whole cavity with all three cells is cooled by large dilution refrigerator (see e.g. [12] for basic principles of its work) with cooling power up to 350 mW (see [13]) which is enough to keep stable temperature around 60 mK with heat input from microwaves during polarization build up and heat input from muon beam during physics data taking.

The target is equiped by several thermometers for monitoring the temperature during both polarization buildup and frozen spin mode (i.e. when the buildup is stopped and polarization is fixed in either transverse mode or longitudinal mode) and also for precise temperature measurement, which is needed during thermal equilibrium calibration. The refrigerator is of course equiped by several flowmeters, pressure gauges and valve controls, it is pretty much standard dilution refrigerator but much larger than standard one.

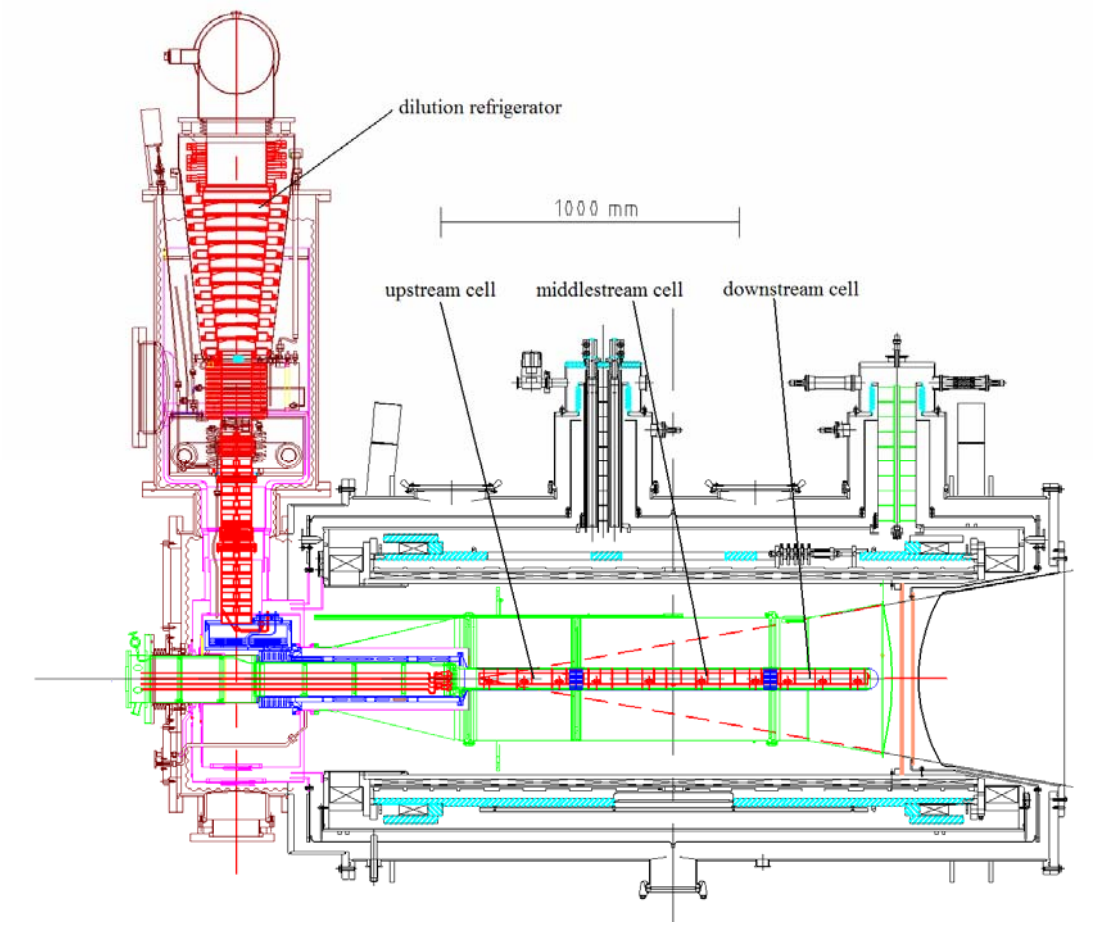

Figure 2.2.1 - Polarized target

The refrigerator is placed in large superconducting magnet cooled by liquid helium. The magnet itself consists of two magnets – 2.5 T solenoid and 0.6 T dipole and both can be used independently. This configuration allows to take data with both transverse and longitudinal polarization (with respect to the beam) and to change the polarization in one direction to polarization of opposite direction without loss of polarization (this mainly concerns longitudinal polarization to reduce systematics of measurement with beam). This can be done by so called field rotation which can be described (roughly speaking) as ramping down one magnet while ramping up the second one. At the moment when the first magnet is ramped down the second is already ramped up. Then this can be started in oposite way and at the end magnetic field has oposite direction than before and because there is no time period without field the polarization is preserved. The magnet is equiped with 16 trim coils to increase homogenity of the field to allow the polarization buildup (which needs rather homogenous field) and also the NMR measurement of the polarization.

For the measurement of the polarization the continuous NMR is used. Fig.2.2.2 (with small modifications taken from [10]) shows the schematics of the NMR system. The so called Yale-cards (DC offset cards) are used mainly for amplification, where the nominal gain can be set as 1 or 207, first is used during DNP and second one is used during TE calibration. Data acquisition is controlled by LabView program.

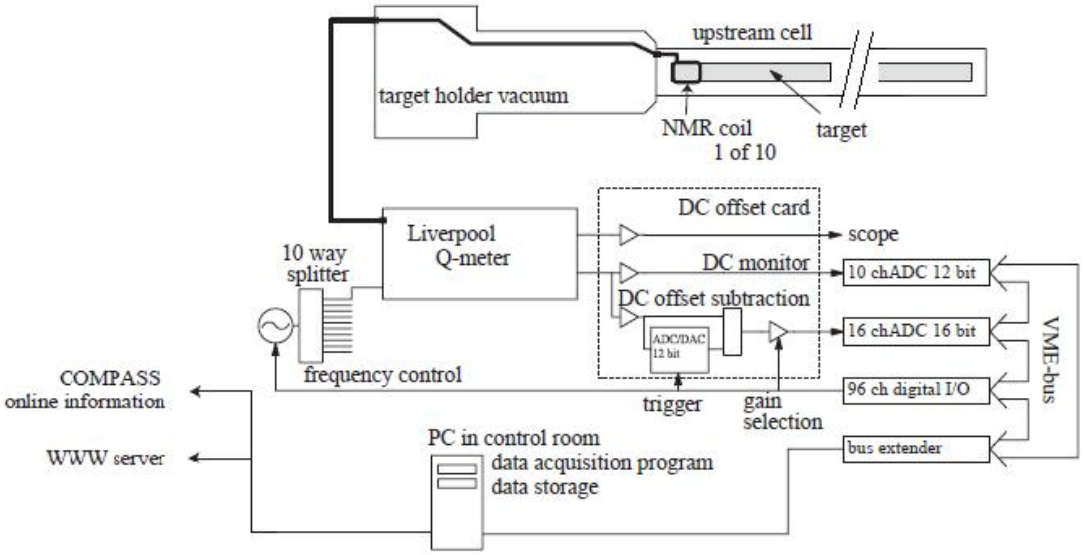

Figure 2.2.2 NMR system

The amonnia used as target material is in form of small spheres with approximately 3 to 4 mm in diameter. This material is iradiated to contain paramagnetic centers (which allow dynamic nuclear polarization) on synchrotron in Bochum.

3. Polarization analysis

3.1. General procedure

As was shown in section 1.3. the polarization is proportional to area under the NMR signal and polarization at thermal equilibrium can be exactly calculated by formula (1.2.5). These two facts actually pretty much say how to determine polarization of the target. Let's look at typical NMR signal shown in fig. 3.1.1.

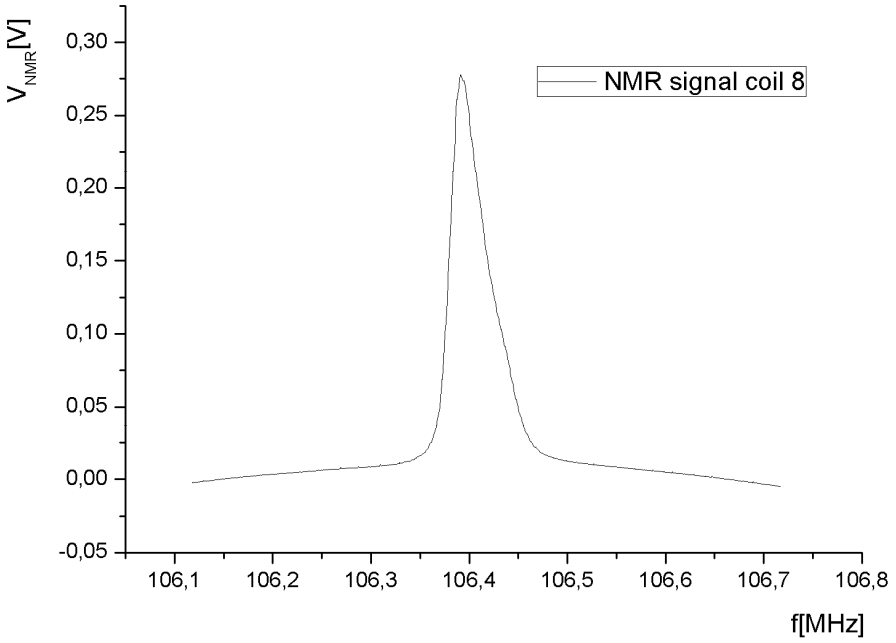

Figure 3.1.1 - NMR signal from June 17

As can be seen first thing one must do is to subtract the background. Then we obtain signal which is look like the one shown in fig. 3.1.2. Generally the signal is shifted, so it is necessary to fit the off-resonance region by linear function and subtract this linear baseline. (Sometimes it might be better to use parabolic fit.) After these two steps all which remains is to integrate the area. This of course must be done for each coil. Now we can obtain polarization value by using the simple formula (1.3.9). All we need is calibration constant.

One could naively use same procedure to obtain the area, then calculate TE (thermal equilibrium) polarization by formula (1.2.5) and by using formula (1.3.10) obtain the calibration costant. This is unfortunately not so easy. The complication has

actually two reasons. First is that the signal of TE calibration is rather small. Well, the size of measured signal is pretty much the same as in case of dynamic polarization, but one must not forget that the TE signal is more than 200 times amplified. This of course leads to signal which is much noisier, which means that the fitting of linear baseline leads to different integrated area, depending on choice of fitting region. Second problem is that because of the smallness of the raw signal, more than just target material may contribute to it. As a result of this TE signal measurement of empty target is always done after finishing the run, usually in November. Now, this empty TE signal is really much smaller than the ordinary TE signal (as will be shown in following sections) and needs special treatment too.

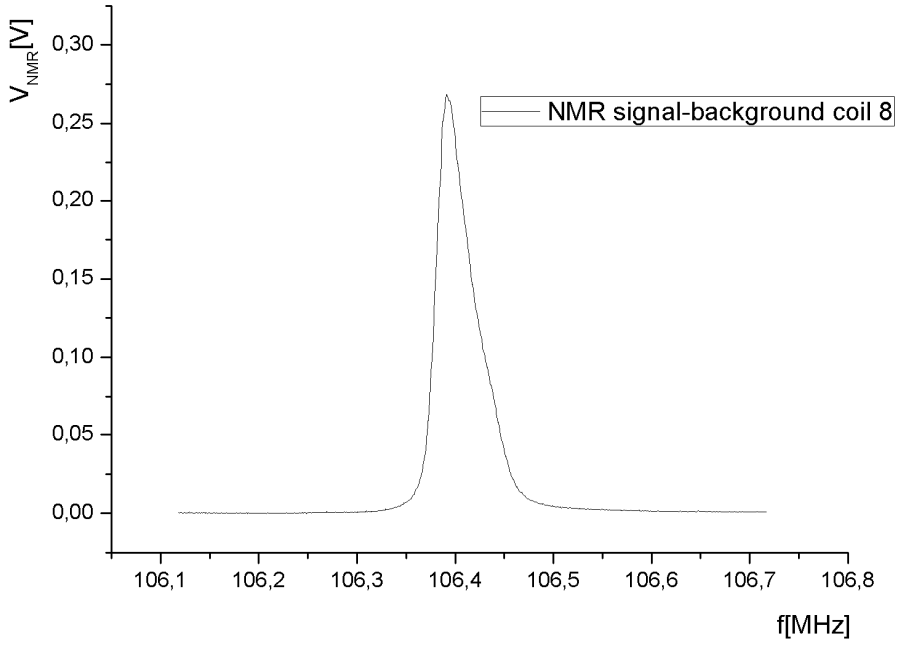

Figure 3.1.2 - NMR signal with background subtracted

As was said in previous paragraph the resulting integrated area of a small signal depends largely on the choice of fitting region of the linear baseline. The most straightforward solution of this problem is probably to select many fitting regions for one signal, integrate area for all of them and then just average the resulting areas. One could probably choose some more sophisticated statistical treatments, but as was shown in [14] the results obtained by different and more complicated methods leads to same results. (Or more precisely – to results which are the same within their

uncertainities.) The specific selection of the fitting region will be shown in next section.

So, let's suppose that we have the precise integrated areas of TE signals. Unfortunately this is still not the end of the story. The TE calibration is ussualy done for three different temperatures. If one determined the calibration constants by the procedure described above, one could also obtain three different results. What is ussually calculated are the so called Curie constants, which are those constants which appear in the Curie law described by formula (1.3.11). These are obtained simply by fitting the obtained areas for all three temperatures by Curie law. The Curie constant the coresponds exactly to the area of TE signal at 1 K. With the knowledge of the gains of amplifier for all coils which are used, calibration constants can be calculated very easily.

3.2. Overview of run 2010

This section will give datailed description of 2010 run. It's quite clear that most of the information presented here have only few quotable sources mainly COMPASS polarized target ELOG [15] and Minutes from weekly meetings of PT group [16], but this is available for collaboration members only (login is needed).

The run (from viewpoint of polarized target) started on 2nd April 2010 by empty TE calibration at three different temperatures of 1.0K, 1.3K and 1.5K. TE calibration followed on 16th April and was done at temperatures of 1.0K, 1.2K and 1.4K. Beam started on 10th May and first polarization buildup started on 18th May in configuration --- (this denotes sign of polarization of upstream, middlestream and downstream cell). Beam ended on 22nd November. After that unloading of material followed on 24th November and empty TE calibration was done at 1.1K and 1.4K.

There were no serious issues with target during whole run. Some issues concerns mainly TE calibration (see [16]). I will discuss it very briefly. Because of faulty Yale card in NMR system some of the NMR signals for coil 1 and 10 were found to be completely useless. Also the temperature reading by two different thermometers was not consistent during 1.4K empty TE calibration. These data were not used, but some discusion still remains in PT group.

3.3. Analysis of 2010 data

After elimination of useless NMR data mentioned above, TE calibration analysis was done according to general description given in section 3.1. All signals were integrated. Empty TE areas and TE areas for all temperatures were fitted by Curie law and thus Curie constant were obtained. These are presented in Tab. 3.3.1. along with final proton signal Curie constants. These are actually obtained simply by subtracting TE constants and empty TE constants. The Curie fits for loaded TE calibration are ploted in Fig.3.3.1 and empty TE Curie fits are plotted in Fig. 3.3.2. Final calibration constants determined from Curie constants, gains for all coils (which are given in [16]) and TE polarization at 1 K determined by formula (1.2.5) are presented in Tab. 3.3.2. Uncertainties are given by statistics and fitting and also by uncertainties of TE temperatures (see [17] for details of handling uncertainties).

Table 3.3.1 - Curie constants

Coil number	Empty TE	Loaded TE	Loaded-empty
1	-3,73±0,16	-6,83±0,11	-3,10±0,20
2	-4,37±0,15	-22,37±0,31	-18,00±0,35
3	-4,59±0,07	-16,90±0,11	-12,31±0,13
4	5,49±0,16	-20,40±0,21	-14,91±0,26
5	-5,23±0,10	-15,09±0,18	-9,86±0,20
6	-4,29±0,11	-19,25±0,08	-14,96±0,13
7	-2,70±0,10	-17,34±0,14	-14,64±0,17
8	-3,62±0,12	-16,86±0,14	-13,24±0,18
9	-4,58±0,08	-15,36±0,17	-10,77±0,18
10	-6,46±0,21	-25,77±0,20	-19,31±0,29

Table 3.3.2 - Calibration constants

Coil number	Gain	Calibration constant
1	213,8	-17,5±1,1
2	213,8	-3,01±0,06
3	213,2	-4,39±0,05
4	214,4	-3,64±0,06
5	211,3	-5,43±0,11
6	213,7	-3,62±0,03
7	217,1	-3,76±0,04
8	214,4	-4,10±0,06
9	215,4	-5,06±0,09
10	212,6	-2,79±0,04

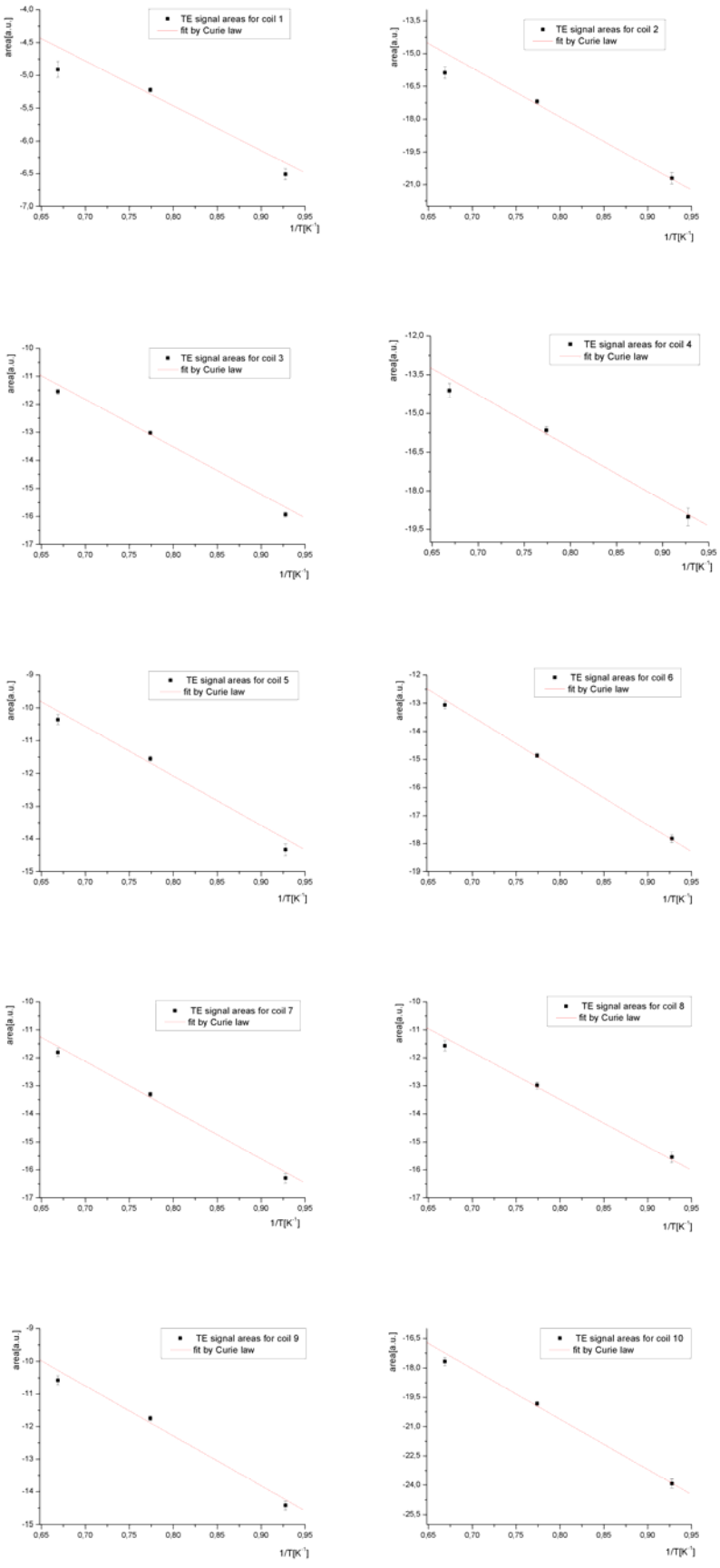

Figure 3.3.1 - Loaded TE Curie fits

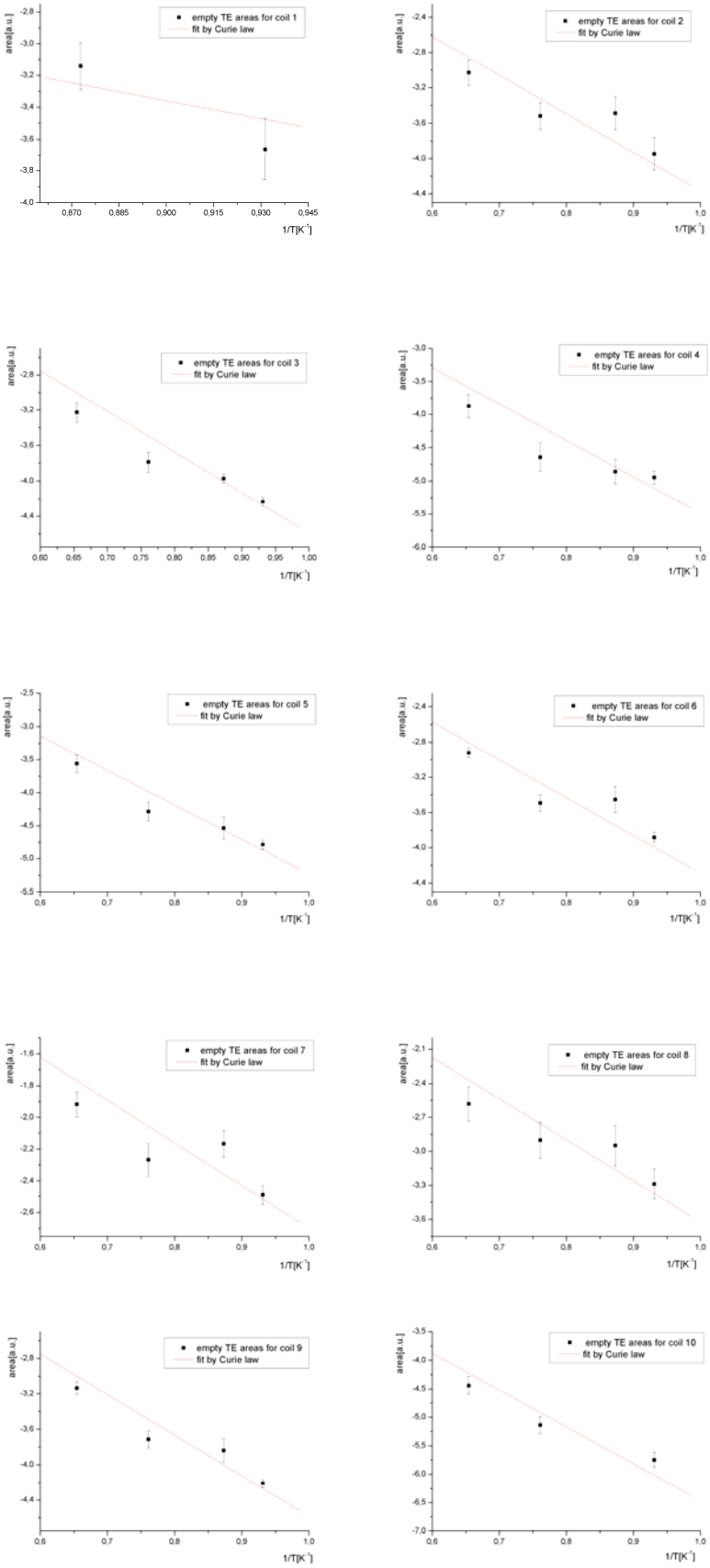

Figure 3.3.2 - Empty TE Curie fits

The polarization buildup data were integrated with excluding 300 kHz region around resonance peak fot the linear baseline fit. The polarization buildup can be plotted for each coil or averaged for each cell. Fig. 3.3.3 shows detail of polarization for 10th June 2010, others are presented in Attachement section. A gap can be clearly seen in the graph. This is due to the unstable LabView application used for NMR data taking which used to crash from time to time resulting in some time without data being taken. Fig. 3.3.4 shows polarization buildup for the whole run 2010 averaged for each cell (this serves for ilustration rather than useful graph). The maximum polarization reached during each polarization buildup is presented in Tab. 3.3.3 along with the day on which the buildup started.

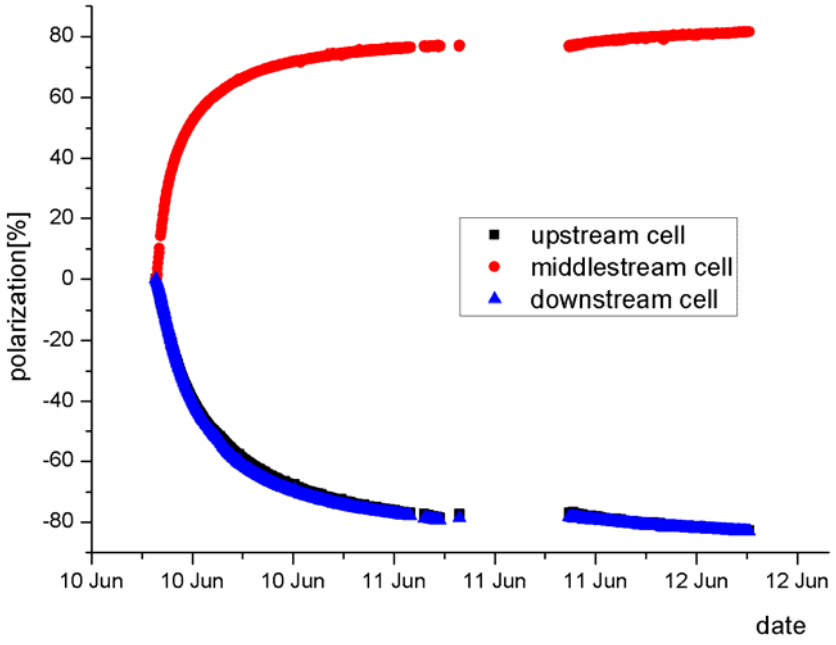

Figure 3.3.3 - Polarization buildup on 10th June

Because polarization was also measured before next polarization buildup, relaxation times can be determined. Because relaxation rates are long, the relaxation can be simply approximated by linear function. Average relaxation rate is $(7,0\pm1,7).10^3\ h$ for upstream cell, $(5,7\pm0,7).10^3\ h$ for middlestream cell and $(5,7\pm1,2).10^3\ h$ downstream cell.

Table 3.3.3 - Reached polarization

Date	Upstream[%]	Middlestream[%]	Downstream[%]
18th May	-43,2±1,4	-0,31±0,01	-49,52±0,75
25th May	83,6±2,6	83,0±1,2	85,4±1,3
27th May	-76,4±2,4	-83,6±1,2	-84,4±1,3
10th June	-82,7±2,6	81,5±1,2	-83,0±1,3
15th June	83,1±2,6	-81,2±1,2	83,0±1,3
23rd June	85,0±2,7	-82,9±1,2	83,5±1,3
26th June	-78,6±2,5	78,9±1,2	-78,8±1,2
2nd July	-80,1±2,5	80,7±1,2	-80,2±1,2
5th July	77,7±2,4	-76,3±1,1	79,1±1,2
8th July	80,9±2,5	-78,5±1,2	81,2±1,2
13th July	-79,2±2,5	80,4±1,2	-78,8±1,2
16th July	-69,2±2,2	74,0±1,1	-73,1±1,1
22nd July	85,5±2,7	-84,3±1,2	83,5±1,3
28th July	85,1±2,7	-83,4±1,2	82,9±1,3
30th July	-80,4±2,5	80,2±1,2	-80,8±1,2
11th August	81,6±2,6	-80,3±1,2	79,7±1,2
17th August	83,9±2,6	-81,6±1,2	82,1±1,3
23rd August	-78,6±2,5	79,2±1,2	-79,0±1,2
1st September	-84,8±2,7	84,2±1,2	-84,1±1,3
10th September	83,4±2,6	-80,7±1,2	81,1±1,2
23rd September	-80,1±2,5	80,3±1,2	-80,5±1,2
6th October	80,0±2,5	-77,3±1,1	80,1±1,2
17th October	-79,6±2,5	81,6±1,2	-79,9±1,2
19th October	-84,7±2,6	84,0±1,2	-85,4±1,3
27th October	81,7±2,6	-79,2±1,2	81,7±1,2
10th November	-77,5±2,4	78,1±1,1	-78,0±1,2
15th November	-83,4±2,6	84,2±1,2	-83,0±1,3

One can clearly see that relative errors are around 3% for the upstream cell and around 1,4% for the middle and downstream cells. The somewhat larger error for the upstream cell is actually caused by quite large error in determining the calibration constant for the first coil, which is caused by errors in the Curie constant, where the empty calibration has fewer points and thus lower statistics and the loaded calibration, where was discovered after the run, that loading of the material was smaller than in the other coils.

It is also worth mentioning that the small points in Fig.3.3.4 are not some residui but they corresponds to short enhacement of polarization or measurement of polarization before next buildup.

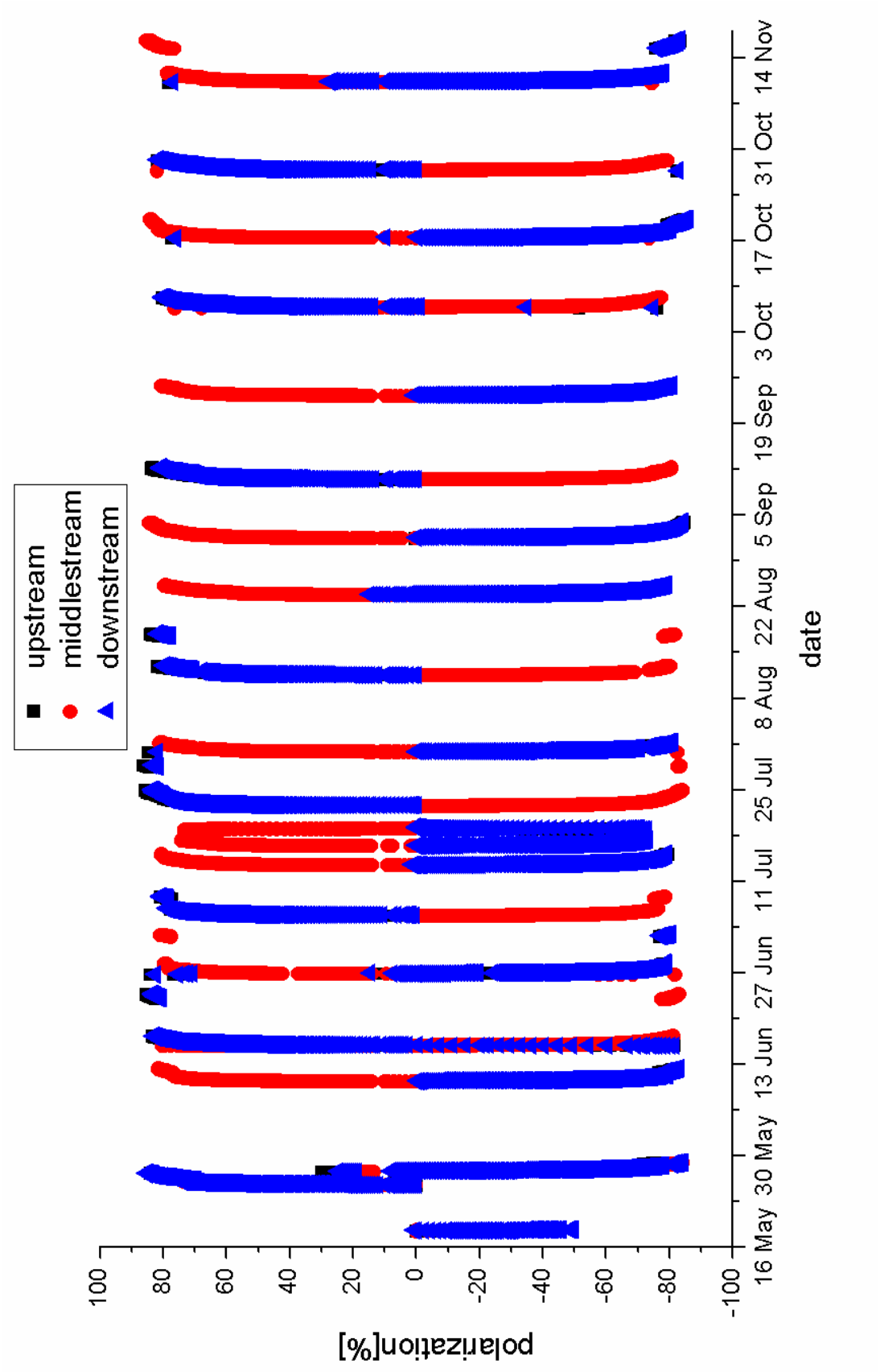

Figure 3.3.4 - Polarization buildup during 2010

3.4. Comparison of results

What should be now of greatest interest is actually comparison of the results obtained in this thesis and the results obtained by the rest of PT group (i.e. Jaakko and Kaori). Tab.3.3.4 shows the Curie constants for empty TE calibration. The absolute difference is also given. There can be clearly seen that Jaakko's and Kaori's constants are systematically somewhat smaller, but as can be seen in the last column the absolute difference is in most cases compatible with zero. (Error is given by sum of constants errors in quadrature.) The same applies for loaded TE calibration, only the differences are larger. Comparison is given in Tab.3.3.5.

The systematic effect can be probably very easily explained, as I have not complete insight in Jaakko's and Kaori's analysis, possibilities are e.g. different regions for baseline fitting or bigger count of them, also the manipulation of the raw data may be explanation, especially elimination of some bad signals, etc.

Table 3.3.4 - Empty TE comparison

Coil number	Thesis	PT group	Difference
1	-3,73±0,16	-3,88±0,27	0,14±0,31
2	-4,37±0,15	-4,54±0,18	0,18±0,24
3	-4,59±0,07	-4,87±0,14	0,28±0,16
4	-5,49±0,16	-6,00±0,18	0,52±0,23
5	-5,23±0,10	-5,61±0,13	0,38±0,16
6	-4,29±0,11	-4,40±0,15	0,11±0,19
7	-2,70±0,10	-2,82±0,16	0,12±0,18
8	-3,62±0,12	-3,85±0,13	0,22±0,18
9	-4,58±0,08	-4,79±0,16	0,21±0,18
10	-6,46±0,21	-6,76±0,26	0,29±0,33

Table 3.3.5 - Loaded TE comparison

Coil number	Thesis	PT group	Difference
1	-6,83±0,11	-6,93±0,12	0,11±0,16
2	-22,37±0,31	-22,82±0,14	0,45±0,34
3	-16,90±0,11	-17,10±0,13	0,20±0,17
4	-20,40±0,21	-20,87±0,32	0,47±0,38
5	-15,09±0,18	-15,40±0,16	0,31±0,24
6	-19,25±0,08	-19,50±0,10	0,25±0,13
7	-17,34±0,14	-17,68±0,14	0,34±0,19
8	-16,86±0,14	-17,28±0,19	0,42±0,23
9	-15,36±0,17	-15,60±0,21	0,25±0,27
10	-25,77±0,20	-26,19±0,24	0,42±0,30

Finally Tab.3.3.6 shows comparison of the Curie constants for the proton signal. As can be expected, the sort of a systematic effect gets cancelled and agrement of the results is almost perfect.

Table 3.3.6 - Proton signal comparison

Coil number	Thesis	PT group	Difference
1	-3,10±0,20	-3,05±0,29	-0,04±0,35
2	-18,00±0,35	-18,27±0,23	0,27±0,42
3	-12,31±0,13	-12,23±0,19	-0,08±0,23
4	-14,91±0,26	-14,86±0,36	-0,05±0,45
5	-9,86±0,20	-9,79±0,21	-0,07±0,29
6	-14,96±0,13	-15,10±0,18	0,14±0,23
7	-14,64±0,17	-14,86±0,21	0,23±0,27
8	-13,24±0,18	-13,43±0,23	0,20±0,29
9	-10,77±0,18	-10,81±0,27	0,04±0,32
10	-19,31±0,29	-19,44±0,35	0,12±0,45

Conclusion

We briefly discussed the basics of inelastic scattering of leptons on nucleons and the importance of polarized target for nucleon structure studies was highlighted. Using the polarized lepton beam and polarized target is actually the only way to study the spin structure of nucleons.

Rather thorough analysis of polarization data measured by continuous NMR technique during run 2010 of COMPASS experiment with transversly polarized target was performed. Maximum reached polarization was around 85% with relative error smaller than 2% (little bit higher, around 3% for upstream cell).

From the measured polarization the relaxation rates for all cells were extracted. Average relaxation rate is $(7,0\pm1,7).10^3$ *h* for upstream cell, $(5,7\pm7,0).10^3$ *h* for middlestream cell and $(5,7\pm1,2).10^3$ *h* downstream cell.

Bibliography

[1] Ashman J. et al.: An Investigation of the Spin Structure of the Proton in Deep Inelastic Scattering of Polarized Muons on Polarized Protons, Nucl. Phys. B328, 1, 1989

[2] Gautheron F. et al.: COMPASS-II Proposal, Geneva, 2010

[3] Bjorken J. D., Paschos E.A., Phys. Rev. 185, 1969, 1975

[4] Devenish R., Cooper-Sarkar A.: Deep Inelastic Scattering, Oxford university press, 2004

[5] Takabayashi N.: Polarized target for the measurement of the gluon contribution to the nucleon spin in the COMPASS experiment, Nagoya, 2003

[6] Abragam A.: The principles of nuclear magnetism, Oxford University Press, 1978

[7] Cejnar P.: Essential Formulae, Prague, 2012

[8] Skrbek L. a kol.: Fyzika nízkých teplot I. část, MatFyzpress, 2011

[9] Kittel Ch.: Introduction to Solid State Physics, John Wiley & Sons, 1996

[10] Kondo K. et al.: Polarization measurement in the COMPASS polarized target, NIMA 526, 70-75, 2004

[11] Abbon P. et al.: The COMPASS experiment at CERN, NIMA 577, 455-518, 2007

[12] Skrbek L. a kol.: Fyzika nízkých teplot II. část, MatFyzpress, 2011

[13] Berglund P. et al.: Dilution refrigerator for COMPASS polarized target, NIMA 498, 101-111, 2003

[14] Lorente-Garcia I.: Data analysis for Compass Polarized target, Geneva, 2004

[15] Polarized Target Elog http://wwwcompass.cern.ch/elog/target_polar/

[16] Koivuniemi J. H.: Minutes from weekly meetings 2010 http://wwwcompass.cern.ch/compass/detector/target/Minutes/2010/

[17] Englich J.: Úvod do praktické fyziky I, MatFyzpress, 2005

List of Tables

List of Figures

Attachment

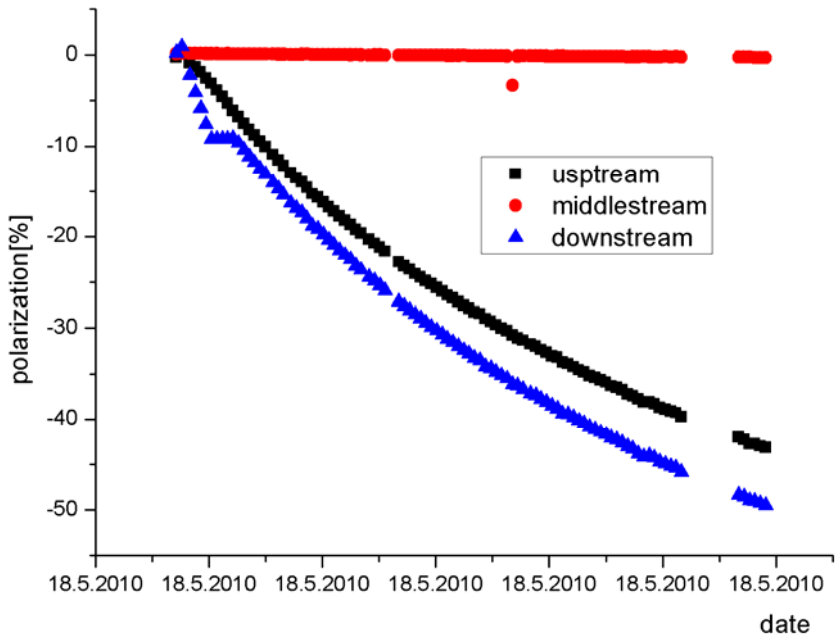

Figure 4.1 Polarization buildup 18.5.2010

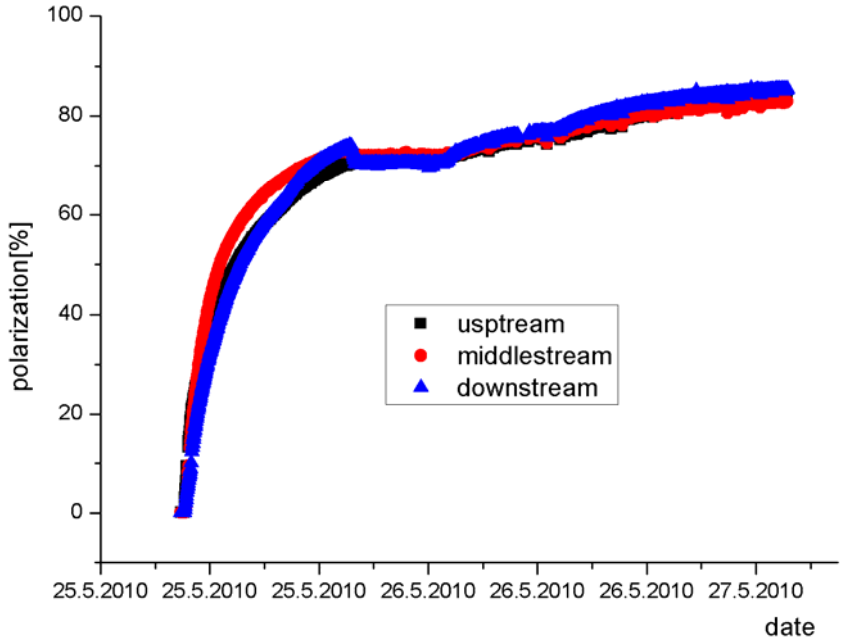

Figure 4.2 Polarization buildup 25.5.2010

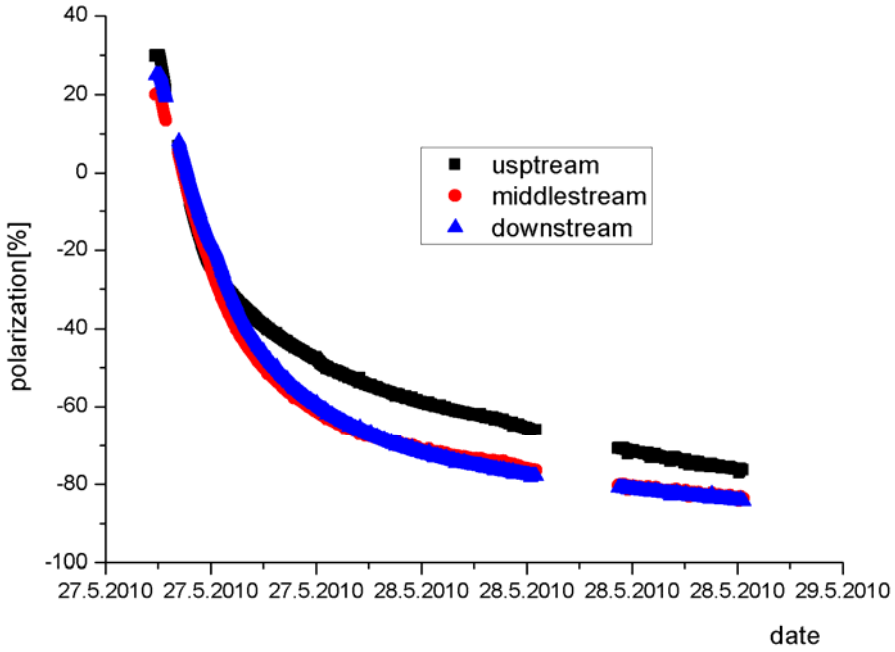

Figure 4.3 Polarization buildup 27.5.2010

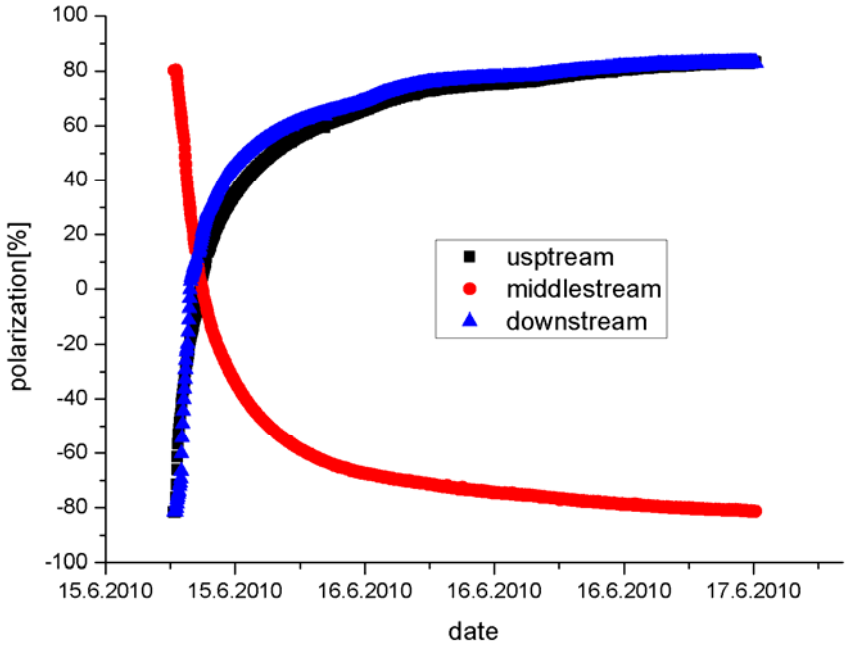

Figure 4.4 Polarization buildup 15.6.2010

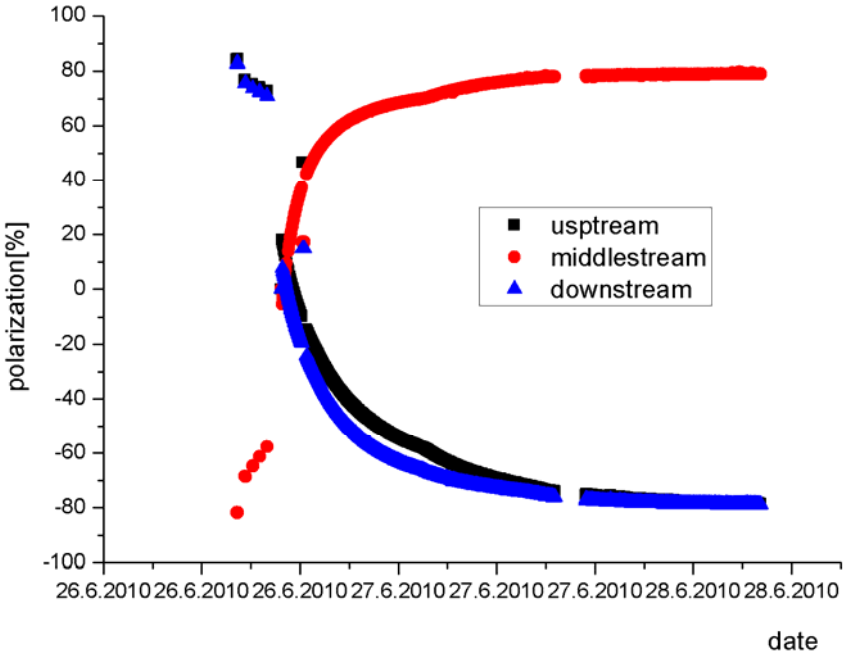

Figure 4.5 Polarization buildup 26.6.2010

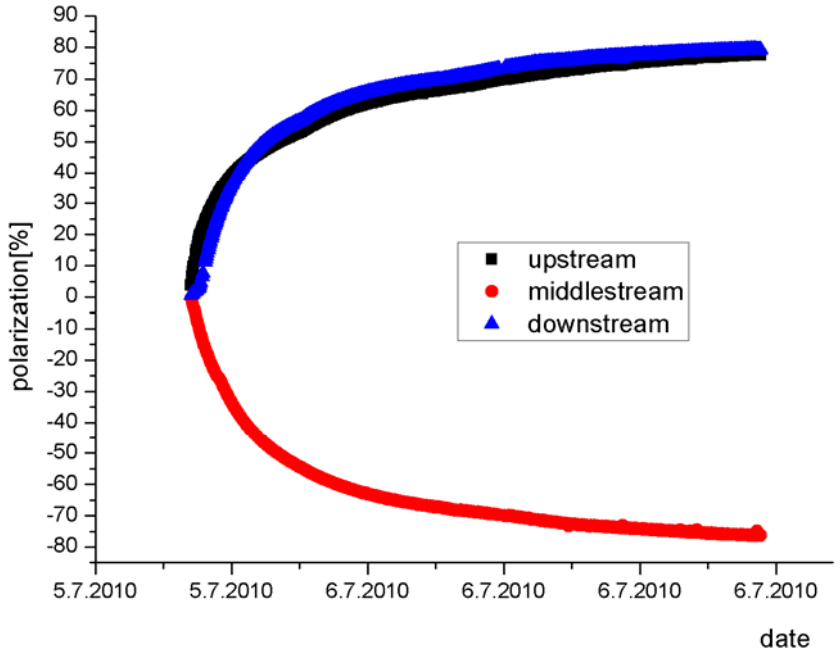

Figure 4.6 Polarization buildup 5.7.2010

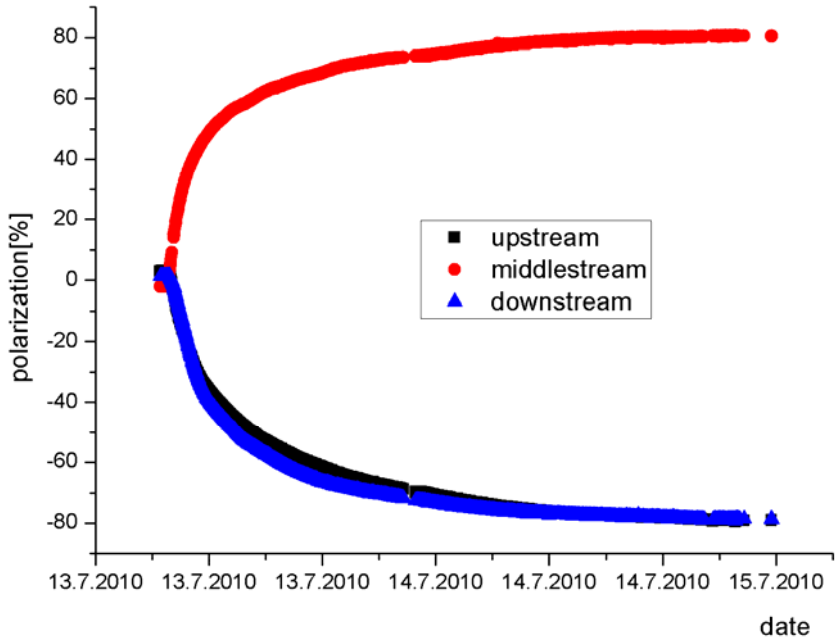

Figure 4.7 Polarization buildup 13.7.2010

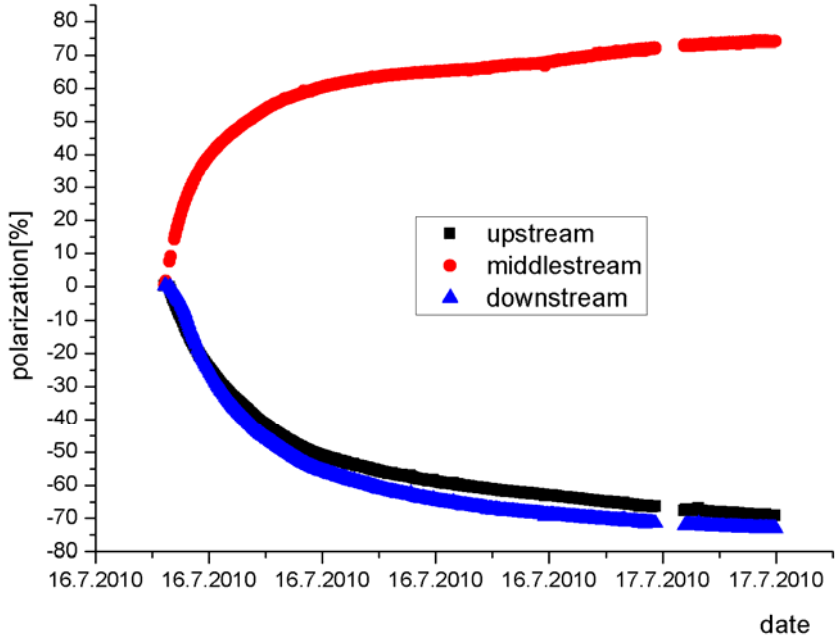

Figure 4.8 Polarization buildup 16.7.2010

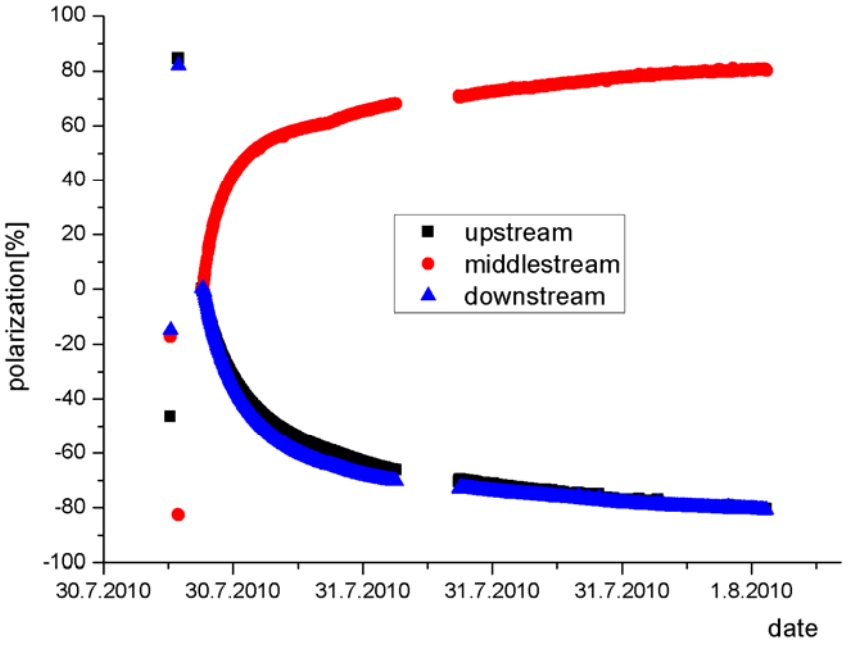

Figure 4.9 Polarization buildup 30.7.2010

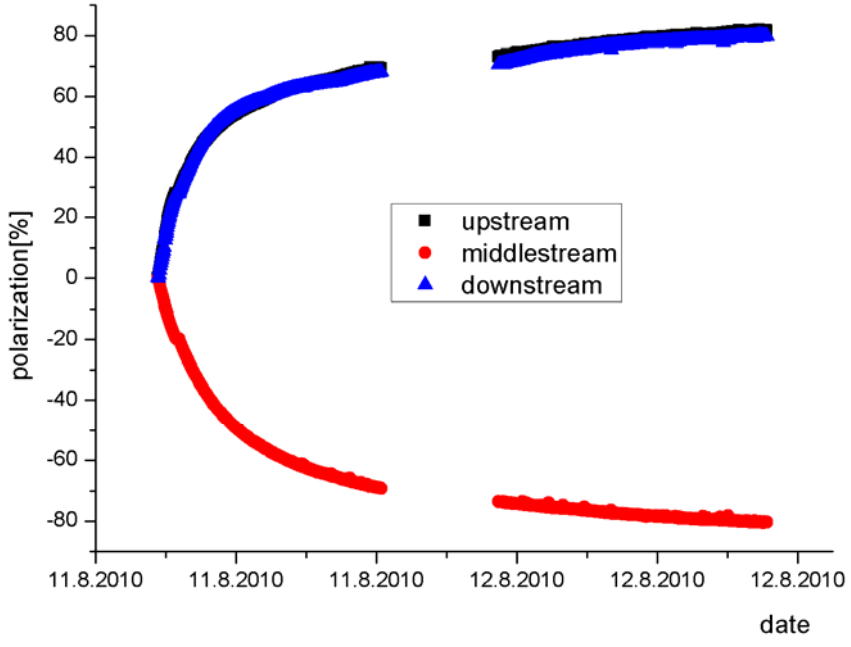

Figure 4.10 Polarization buildup 11.8.2010

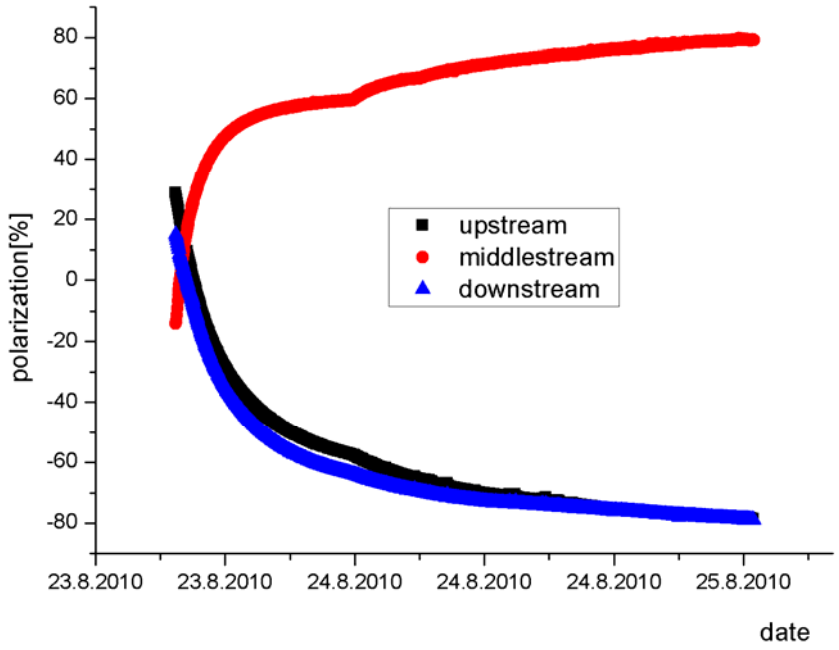

Figure 4.11 Polarization buildup 23.8.2010

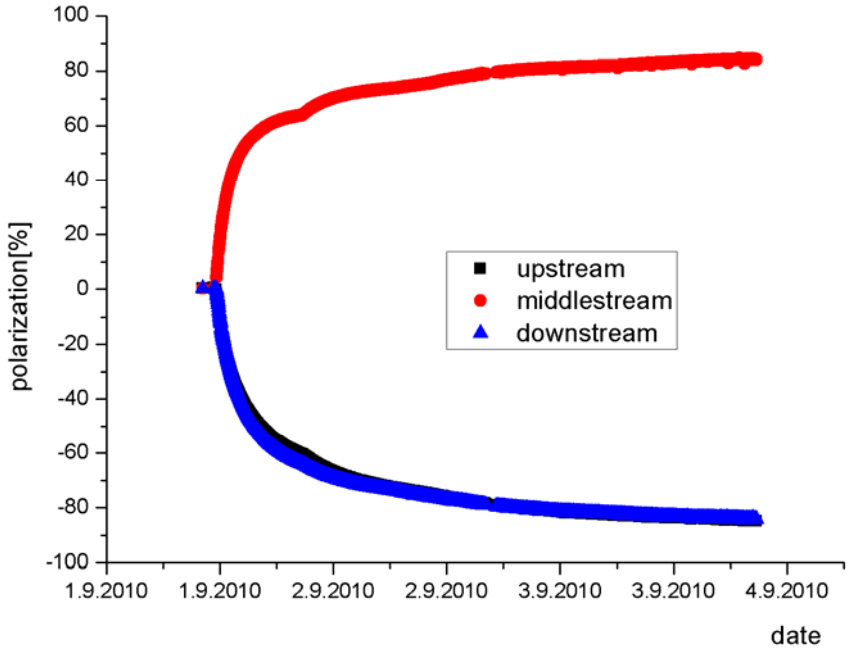

Figure 4.12 Polarization buildup 1.9.2010

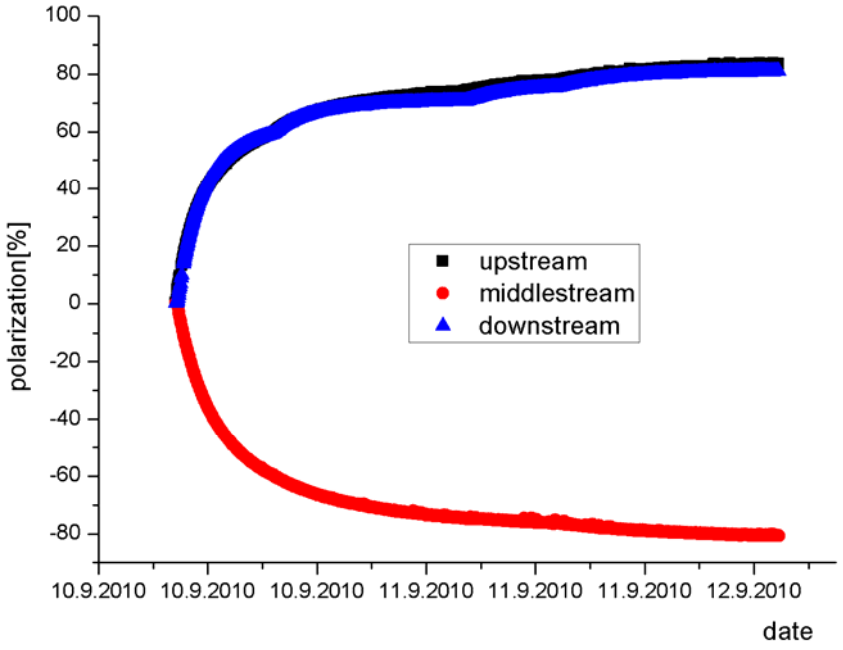

Figure 4.13 Polarization buildup 10.9.2010

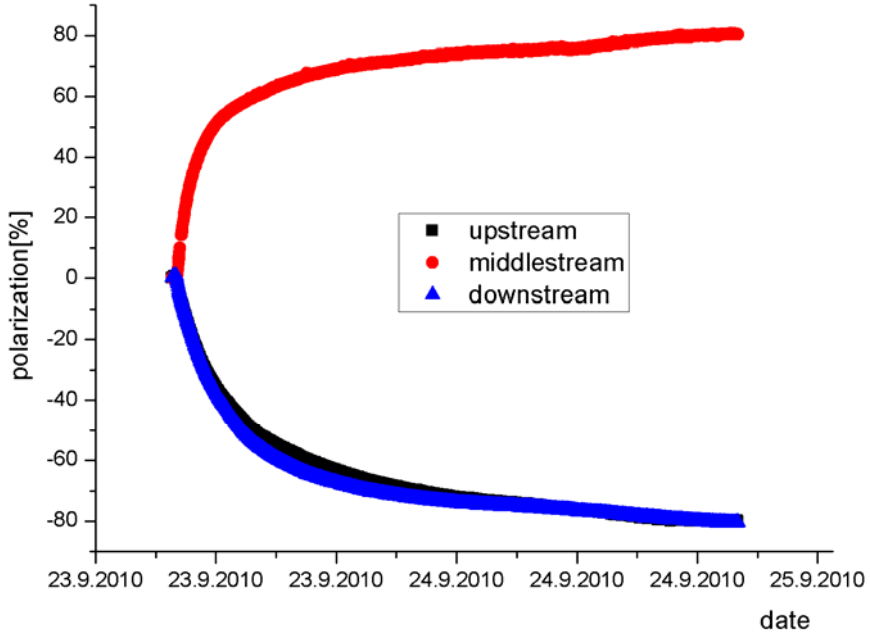

Figure 4.14 Polarization buildup 23.9.2010

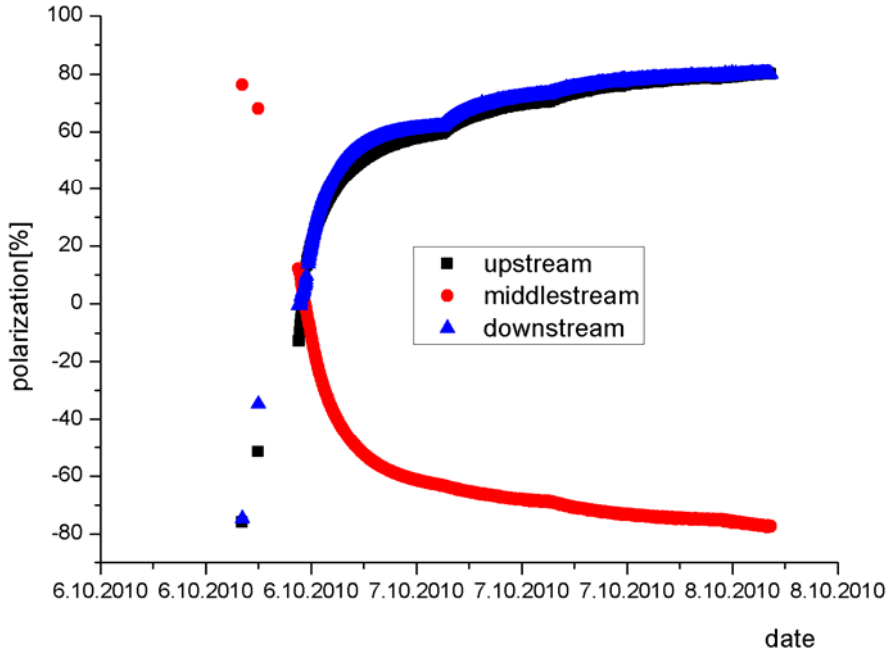

Figure 4.15 Polarization buildup 6.10.2010

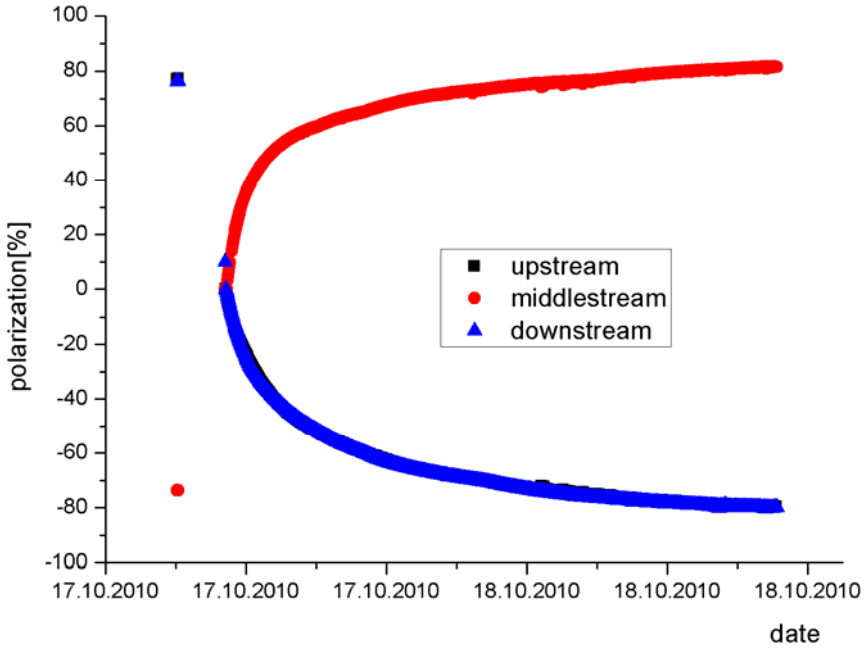

Figure 4.16 Polarization buildup 17.10.2010

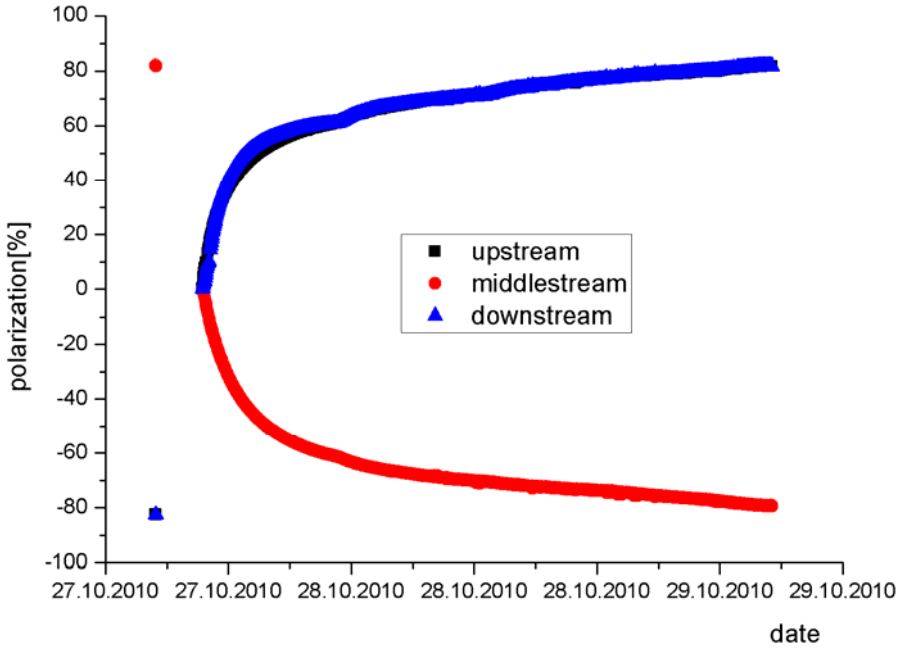

Figure 4.17 Polarization buildup 27.10.2010

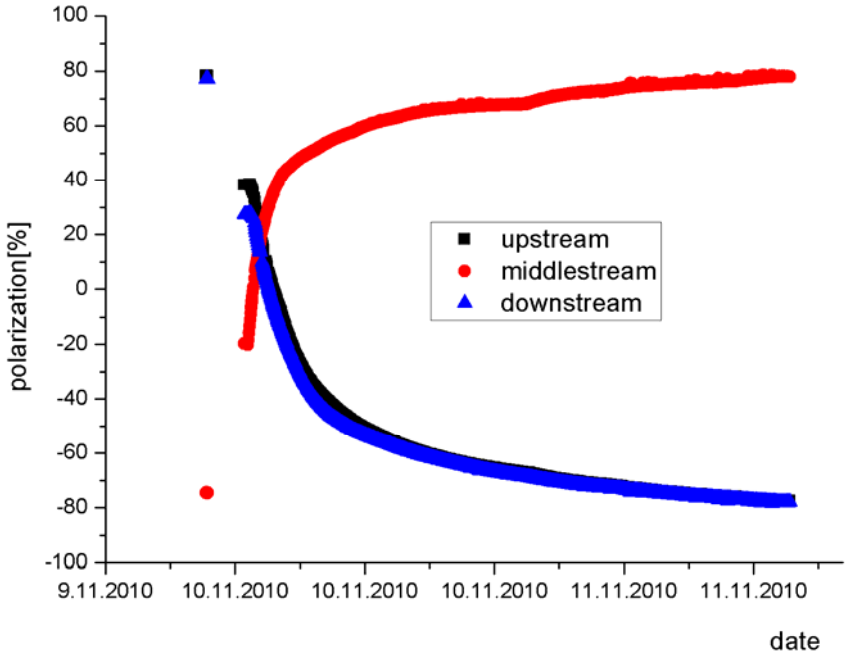

Figure 4.18 Polarization buildup 10.11.2010